Low-mass stars and star clusters in the dark Galactic halo

E.J. Kerins

Observatoire de Strasbourg, 11 Rue de l'Université, F-67000 Strasbourg, France.

arXiv:astro-ph/9704179v2 7 Aug 1997

Abstract. In a previous study it was proposed that the Galactic dark matter being detected by gravitational microlensing experiments such as MACHO may reside in a population of dim halo globular clusters comprising mostly or entirely low-mass stars just above the hydrogen-burning limit. It was shown that, for the case of a standard isothermal halo, the scenario is consistent not only with MACHO observations but also with cluster dynamical constraints and number-count limits imposed by 20 Hubble Space Telescope (HST) fields. The present work extends the original study by considering the dependency of the results on halo model, and by increasing the sample of HST fields to 51 (including the Hubble Deep Field and Groth Strip fields). The model dependency of the results is tested using the same reference power-law halo models employed by the MACHO team. For the unclustered scenario HST counts imply a model-dependent halo fraction of at most $0.5 - 1.1\%$ (95% confidence), well below the inferred MACHO fraction. For the cluster scenario all the halo models permit a range of cluster masses and radii to satisfy HST, MACHO and dynamical constraints. Whilst the strong HST limits on the unclustered scenario imply that at least 95% of halo stars must reside in clusters at present, this limit is weakened if the stars which have escaped from clusters retain a degree of clumpiness in their distribution.

Key words: stars: low-mass, brown dwarfs – globular clusters: general – Galaxy: halo – dark matter

1. Introduction

The abundance and nature of dark matter in the halo of our Galaxy is rapidly making the transition from theoretical hypothesis to observational science. This has been facilitated by the deep surveys that are now achievable with instruments such as the Hubble Space Telescope (HST)

and by several gravitational microlensing searches that are currently in progress.

The 2nd-year results from the MACHO microlensing experiment (Alcock et al. 1997) towards the Large Magellanic Cloud (LMC), a direction which is sensitive to lenses residing in the dark halo, indicate that a substantial fraction of the halo $(20 - 100\%)$ comprises objects with a typical mass in the range $0.1 - 1$ M$_\odot$.[1] These results appear to be broadly supported by the provisional findings from 4 years of MACHO observations (Axelrod 1997) which have uncovered at least 14 LMC microlensing candidates. Similar mass scales have also been implicated by the EROS I microlensing experiment (Renault et al. 1997), though with a somewhat lower inferred halo fraction. These results are consistent with the lenses being in the form of low-mass hydrogen-burning stars or white-dwarf remnants.

However, both of these candidates appear unattractive when other observational and theoretical results are taken into consideration. The number density, age and mass function of white dwarfs in the Galaxy is strongly constrained by number counts of high-velocity dwarfs in the Solar neighbourhood, and by their helium production (Carr et al. 1984; Ryu et al. 1990; Adams & Laughlin 1996; Chabrier et al. 1996; Graff et al. 1997). In particular, Chabrier et al. (1996) find that a halo fraction compatible with MACHO results requires that white dwarfs be older than 18 Gyr, though more recently Graff et al. (1997) have argued for a lower limit closer to 15.5 Gyr based upon reasonable white-dwarf model assumptions and a halo fraction of 30%. The situation for low-mass stars appears at least as pessimistic with recent HST results indicating that a smoothly distributed population of low-mass stars can contribute no more than a few percent to the halo dark matter density, regardless of stellar metallicity (Bahcall et al. 1994; Graff & Freese 1996; Flynn et al. 1996; Kerins 1997).

---

[1] This conclusion can be avoided if one instead attributes the observations to lenses residing in a very massive disc, though to explain the MACHO results one requires a local disc column density in excess of that typically inferred from kinematical observations (Kuijken & Gilmore 1989; Bahcall et al. 1992).

It has been suggested (Kerins 1997, hereafter Paper I) that if low-mass stars are clumped into globular-cluster configurations then HST limits can be considerably weakened, since this introduces large fluctuations in number counts and also may prevent a significant fraction of sources within the cores of clusters from being resolved. Motivation for the cluster scenario comes from the predictions of some baryonic dark matter formation theories, which are discussed in Paper I. However, such clusters are required to have masses and radii consistent with existing dynamical constraints on clusters and other massive objects residing in the halo. In Paper I it was shown that agreement between HST counts, dynamical limits and the central value for the halo fraction inferred by MACHO (40% for the halo model assumed) is possible if clusters have a mass around 4×10^4 M$_\odot$ and radius of a few parsecs. However, HST, MACHO and dynamical limits are all dependent upon the unknown halo distribution function, so these results are valid only for the spherically-symmetric, cored isothermal halo model adopted in Paper I.

In this paper the model dependency of such conclusions is investigated using the same set of reference halo models employed in the MACHO collaboration's analysis of its results. One of these models is similar, though not identical, to the model investigated in Paper I, whilst the other models are constructed from the self-consistent set of 'power-law' halo models presented by Evans (1994). All models are normalised to be consistent with observational constraints on the Galactic rotation curve and local column surface density. New data from the Hubble Deep Field (Flynn et al. 1996) and Groth Strip (Gould et al. 1997) are also incorporated, as well as two other new fields analysed by Gould et al., extending the analysis from 20 HST fields in Paper I to 51 in this study.

2. Halo models

In Paper I constraints on the halo fraction in clustered and unclustered low-mass stars are derived assuming the stars have zero metallicity and that the halo density ρ varies with Galactocentric cylindrical coordinates (R, z) as

$$\rho = \rho_0 \left(\frac{R_c^2 + R_0^2}{R_c^2 + R^2 + z^2} \right) \tag{1}$$

where, in Paper I, the local density $\rho_0 = 0.01$ M$_\odot$ pc^{-3}, the Solar Galactocentric distance $R_0 = 8$ kpc, and the halo core radius $R_c = 5$ kpc.

The assumption of zero metallicity is maintained in the present analysis since one expects the halo to be perhaps the oldest of the Galactic components, and hence its constituents to have more or less primordial metallicity. The expected absolute magnitude in various photometric bands for such stars between the hydrogen-burning limit mass (0.092 M$_\odot$) and 0.2 M$_\odot$ has been calculated

by Saumon et al. (1994) and their results are employed here as in Paper I.

The model dependency of the conclusions in Paper I is assessed by re-calculating the constraints for a number of different, but plausible, halo models. For ease of comparison the models selected are 5 of the reference halo models used by the MACHO collaboration (Alcock et al. 1996) in its analysis. (MACHO considers a total of 8 Galactic models, though only 5 of the halo models have distinct functional forms.) All halo models assume $R_0 = 8.5$ kpc and $R_c = 5$ kpc. The 5 models are denoted by MACHO as models A–D and S (for 'standard'), and this labelling is maintained here.

The standard model S has the same functional form as the halo investigated in Paper I (i.e. it is described by Eq. 1) but uses the slightly larger IAU value for R_0 above and assumes a lower local density $\rho_0 = 0.0079$ M$_\odot$ pc^{-3}. Models A–D are drawn from the self-consistent family of power-law models (Evans 1994), having density profiles

$$\rho = \frac{v_a^2 R_c^\beta}{4\pi G q} \frac{R_c^2(1 + 2q^2) + R^2(1 - \beta q^2) + z^2[2 - q^{-2}(1+\beta)]}{(R_c^2 + R^2 + z^2 q^{-2})^{(\beta+4)/2}}, \tag{2}$$

where v_a is the velocity normalisation, q describes the flattening of equipotentials, β determines the power-law slope of the density profile at large radii, and π and G have their usual meanings. For a flat rotation curve at large radii $\beta = 0$, where as for a rising curve $\beta < 0$ and for a falling one $\beta > 0$.

Table 1. Parameter values for the 5 MACHO reference halo models A–D and S (Alcock et al. 1996). $R_0 = 8.5$ kpc and $R_c = 5$ kpc is assumed for all models. For models A–D the local density ρ_0 is derived from the parameters in columns 2–4. The local rotation speed v_0 is computed from the combined halo and disc mass within R_0.

Model	v_a/km s^{-1}	q	β	ρ_0/M$_\odot$ pc^{-3}	v_0/km s^{-1}
A	200	1	0.0	0.0115	224
B	200	1	-0.2	0.0145	233
C	180	1	0.2	0.0073	203
D	200	0.71	0.0	0.0190	224
S	–	–	–	0.0079	192

The particular parameters for models A–D, along with those of model S are listed in Table 1. Model A is the closest analogy to model S within the power-law family of models, whilst model B has a rising rotation curve at large radii, model C a falling rotation curve, and model D a flattening equivalent to an E6 halo. When combined with the MACHO canonical Galactic disc (Alcock et al. 1996), the models give values for the local Galactic rotation speed v_0 within 15% of the IAU standard value of

220 km s^{-1} and have rotation curves that are consistent with observations.

3. HST observations and halo fraction constraints

Gould et al. (1997) have calculated the disc luminosity function for M-dwarf stars using data from several HST WFC2 fields. These include 22 fields originally analysed by Gould et al. (1996), along with the Hubble Deep Field, 28 overlapping fields comprising the Groth Strip, and 2 other new fields: a total of 53 WFC2 fields. In Paper I, 20 of the original 22 fields are analysed, the other 2 fields being omitted due to statistical problems introduced by their close proximity to some of the other fields (namely that clusters appearing in these fields could also appear in the other fields and thus be double counted). In this study these 20 fields are combined with the new fields analysed by Gould et al. (1997), making the total number of fields 51. The nearest-neighbour separation between these fields is sufficiently large that double counting is not expected to be a problem for clusters of interest. (The overlapping Groth Strip fields are treated as a single large field for the purpose of this study.)

The limiting and saturation I-band magnitudes for the fields are listed in Table 1 of Gould et al. (1997). The Groth Strip is treated as a single field with an angular coverage of 25.98 WFC2 fields (this accounts for overlaps) and magnitude limits corresponding to the modal values listed in Gould et al. (1997). As in Paper I, these limits are translated into star-mass dependent limiting distances by converting the line-of-sight extinction values listed in Burstein & Heiles (1984) to I-band reddenings and using the photometric predictions of Saumon et al. (1994) for zero-metallicity low-mass stars. The predictions for the V and I bands are well fit by the colour–magnitude relation

$$I = -11.45\,(V-I)^2 + 40.7\,(V-I) - 24.5 \qquad (3)$$

for $1.27 \leq V - I \leq 1.57$ (corresponding to $0.2 \geq m/\mathrm{M}_\odot \geq 0.092$).

The analyses for the unclustered and clustered scenarios proceed as in Paper I, except that the models listed in Table 1 of this paper now replace the model used there. The calculations for the cluster scenario, which are described in detail in Paper I, assume that the surface-brightness profiles of the clusters follow the King (1962) surface-brightness law and take into account cluster resolvability, as well as line-of-sight overlap.

Table 2 lists the results for the unclustered scenario. Within the 51 HST WFC2 fields analysed a total of 145 candidate stars with $1.2 \leq V - I \leq 1.7$ are found, implying a 95% confidence level (CL) upper limit on the average number of 166 stars. This colour range spans the $V - I$ colour predictions of Saumon et al. (1994) for stars with masses in the interval $0.092 - 0.2\,\mathrm{M}_\odot$, where the lower value corresponds to the hydrogen-burning limit. Comparison with the expected number tabulated in Table 2

Table 2. Constraints on unclustered zero-metallicity low-mass stars in the Galactic halo arising from the detection of 145 candidate stars within 51 HST WFC2 fields. The second and third columns give the expected number of detectable stars N_{exp} for a full halo ($f_{\mathrm{h}} = 1$) for stars with masses of 0.2 M$_\odot$ and 0.092 M$_\odot$ (the hydrogen-burning limit mass), respectively. The last two columns give the 95% confidence upper limit on the maximum halo fraction f_{max}.

| | N_{exp} | | f_{max} | |
Model	0.2 M$_\odot$	0.092 M$_\odot$	0.2 M$_\odot$	0.092 M$_\odot$
A	183 000	24 100	9×10^{-4}	0.007
B	248 000	30 800	6×10^{-4}	0.005
C	109 000	15 000	0.0015	0.011
D	162 000	34 300	0.0010	0.005
S	141 000	17 100	0.0012	0.010

clearly shows that, for all models, even the lowest mass unclustered stars fall well short of providing the halo dark matter density inferred by MACHO. The upper limit on their fractional contribution f_{max} is shown for 0.2-M$_\odot$ and 0.092-M$_\odot$ stars. For the lowest mass stars f_{max} ranges from 0.5% for models B and D to 1.1% for the lighter halo model C.

One interesting feature of Table 2 is that for the flattened halo model D the expected number counts are enhanced for 0.092-M$_\odot$ stars relative to the predictions for the spherically symmetric models, producing the highest predicted number-count for these stars. This contrasts with the results for the brighter 0.2-M$_\odot$ stars, with the heavy halo model B producing the highest number-count prediction. The enhancement for 0.092-M$_\odot$ stars in model D arises because the flattening preferentially increases the stellar surface density near the Galactic plane, and this is reflected in the counts of 0.092-M$_\odot$ stars which can be at most only a few kpc from the plane if they are to be detected.

The constraints on the halo fraction f_{h} for the clustered scenario as a function of cluster mass M and radius R are shown in Fig. 1 for the 5 models (A–D, S) assuming all stars reside in clusters and have the hydrogen-burning limit mass of 0.092 M$_\odot$. Each plot is characterised by a lower plateau to the left, an upper plateau to the right and a curved rising surface joining the two. This curved surface between the two flat regions represents the 95% CL upper limit halo fraction in clusters inferred from the presence of only 145 candidate stars within the 51 HST WFC2 fields. The constraints are actually calculated on the basis of no stars being present within these fields, since for clusters there is little difference in the constraints assuming no stars are found or assuming a few hundred stars are found. The reason for this, as discussed in Paper I, is that the clusters considered here contain between 1000 and 10^7 members each, so the presence of just one cluster within
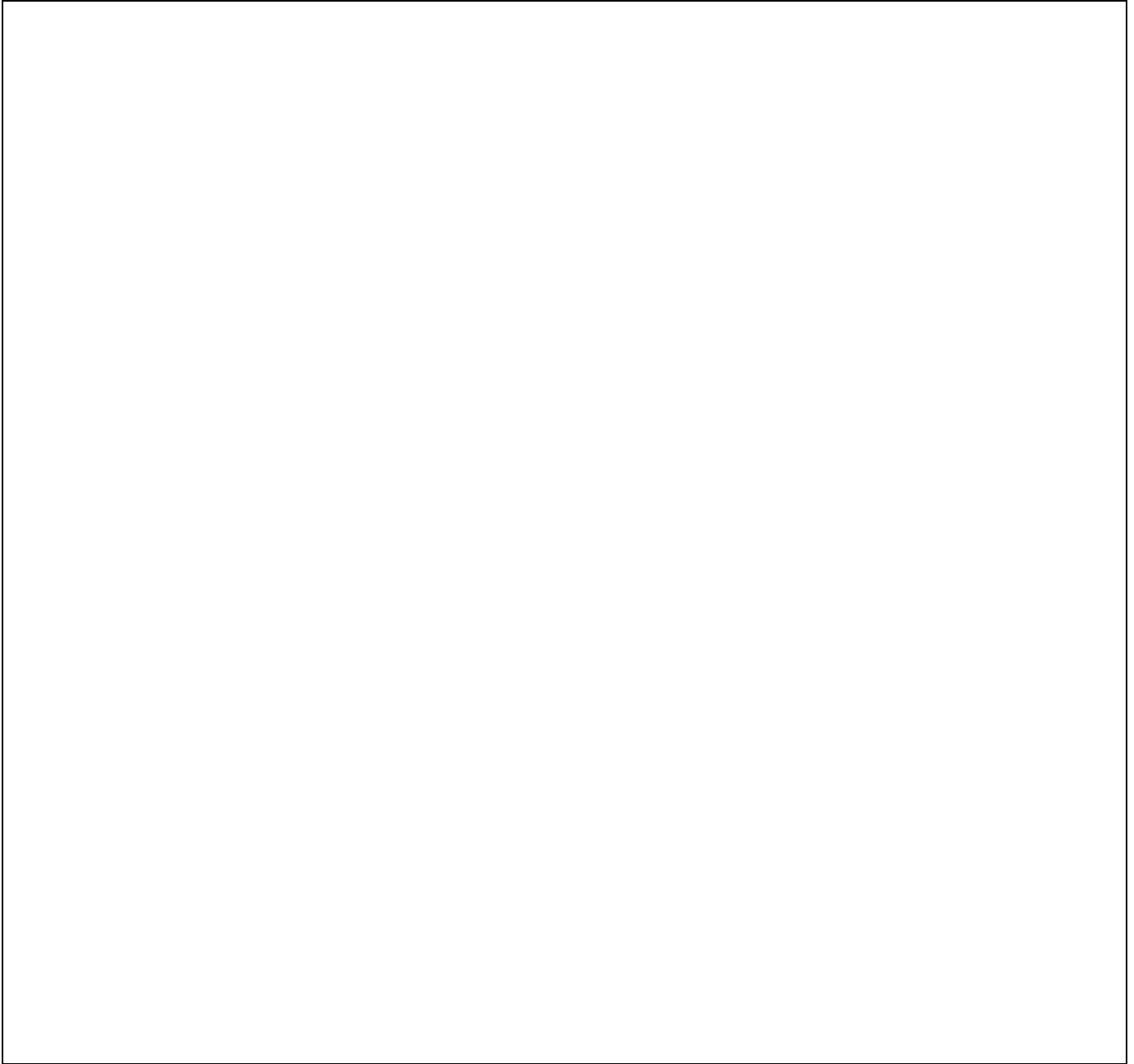
Fig. 1. Comparison of constraints on the halo fraction $f_{\rm h}$ from HST limits, MACHO observations and dynamical constraints for the 5 halo reference models (A–D, S), assuming halo stars have a mass of 0.092 M$_{\odot}$ and all reside in clusters with mass M and radius R. The lower plateau to the left of each plot corresponds to the 95% CL upper limit $f_{\rm max}$ for the unclustered scenario inferred from HST counts (see Table 2). The upper plateau on the right corresponds to the 95% CL lower limit halo fraction $f_{\rm M,low}$ inferred by MACHO 1st- and 2nd-year observations (Alcock et al. 1997), with the central value for the MACHO halo fraction $f_{\rm M}$ indicated by the skirting surrounding the plots (see also Table 3). The curved surface joining the lower and upper flat regions corresponds to the 95% CL upper limit on the halo fraction in clusters from HST counts. Also projected onto the plane $f_{\rm h} = f_{\rm M,low}$ are the cluster dynamical constraints (dashed lines) for the local Solar neighbourhood. The intersection between these constraints and the MACHO lower-limit plateau indicates cluster parameters compatible with HST, MACHO and dynamical constraints.

any of the HST fields would typically result in thousands if not millions of candidates being detected.

The lower plateau shows the 95% CL upper limit halo fraction for the *unclustered* scenario (corresponding to the $f_{\rm max}$ values listed in Table 2). Clusters with masses and radii within this region have internal densities which are lower than that of the halo background average and are thus unphysical, since they represent local under-densities rather than over-densities. Clearly constraints on clusters cannot be stronger than constraints on a smooth stellar distribution. The intersection of the lower plateau with the curved rising surface therefore denotes the boundary between unphysical and physical cluster parameters.
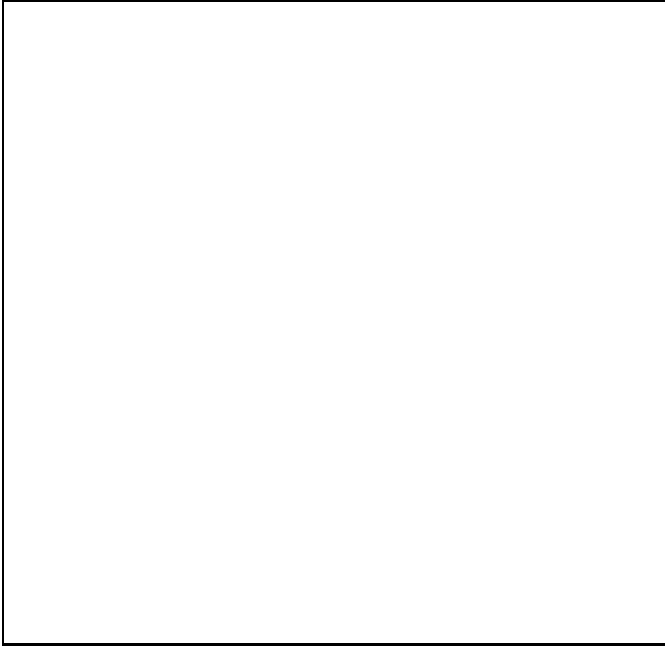

Fig. 1. *continued.*

The upper plateau to the right represents the 95% CL *lower limit* on the halo fraction $f_{\rm M,low}$ inferred from MA-CHO 1st- and 2nd-year microlensing results (Alcock et al. 1997). It is calculated by taking the 95% CL lower limit on the measured microlensing optical depth for all 8 MACHO events ($\tau > 1.47 \times 10^{-7}$), subtracting the optical depth contribution expected from non-halo components [corresponding to $\tau_{\rm non-halo} \simeq 5 \times 10^{-8}$ (Alcock et al. 1996)], and normalising to the optical depth prediction $\tau_{\rm exp}$ for a full halo ($f_{\rm h} = 1$) for each model. The top of the skirting surrounding each plot is normalised to the *central* MA-CHO value for the halo fraction $f_{\rm M}$ for comparison, and is calculated in a similar manner to the lower limit ($f_{\rm M}$ and $f_{\rm M,low}$, together with $\tau_{\rm exp}$, are tabulated in Table 3 for each model). Since this plateau lies below the extrapolation of the HST cluster-fraction constraint [which rises

asymptotically over this region – see Fig. 2 of Paper I], it is consistent with both MACHO and HST limits.

The dashed lines in the plots of Fig. 1 represent the dynamical constraints derived for the local Solar neighbourhood. In fact some of the HST fields are somewhat closer in to the Galactic centre, where the dynamical constraints are stronger, but most are further away so the limits shown are stronger than applicable for most of the HST fields. The functional form for the constraints are detailed in Paper I and are dependent upon Galactic as well as cluster parameters [consult Lacey & Ostriker (1985); Carr & Lacey (1987); Moore (1993); Moore & Silk (1995); Carr & Sakellariadou (1997) for derivations, and see Carr (1994) for a detailed review of dynamical constraints]. Their variation from plot to plot is due to model variations in the local density and rotation speed (see Table 1). The dynamical constraints are projected onto the plane $f_{\rm h} = f_{\rm M,low}$ for direct comparison with the MACHO lower limits. The intersection of the MACHO lower-limit plateau with the dynamical limits therefore represents cluster parameters compatible with MACHO, dynamical limits, and the constraints from the 51 HST fields.

For each model it is evident that the region compatible with all limits spans a significant range of masses and radii. For models C and D the maximum permitted cluster mass is around 5×10^4 M$_\odot$, whilst for models A, B and S one can have cluster masses in excess of 10^6 M$_\odot$. Interestingly, whilst in the unclustered scenario the heavy halo model B is the most strongly constrained in terms of allowed halo fraction $f_{\rm max}$, it nonetheless allows a relatively wide range of viable cluster masses in the clustered scenario. Conversely, the permitted cluster mass range for the light halo model C is more restricted.

This apparent paradox is due to the fact that the HST, dynamical and microlensing observations limit the halo density normalisation at different positions in the halo, so their intersection is sensitive to the halo density profile. In particular, the HST and dynamical limits essentially apply to the local Solar neighbourhood position ($R_0 = 8$ kpc) for clusters comprising relatively dim hydrogen-burning limit stars, where as the microlensing observations towards the LMC constrain the density of lenses at somewhat larger distances (primarily between 10 and 30 kpc from the Galactic centre, where the product of lens number density and lensing cross-section is largest). Hence, for a given microlensing constraint on the mass density of lenses at 10 to 30 kpc, the local dynamical and number-count constraints are weaker for haloes with rising rotation curves (such as model B) than for models with falling rotation curves (such as model C).

The relatively large range in allowed cluster masses and radii for model S is in apparent contrast to the results of Paper I, in which the surviving parameter space is shown to be much smaller for the very similar model adopted there. There are two reasons for this apparent discrepancy: (1) in Fig. 1 of this paper it is assumed that

the clusters comprise hydrogen-burning limit stars, whereas in Fig. 3 of Paper I the constraints are shown for the brighter 0.2-$M_\odot$ stars; (2) in this study consistency is being demanded only with the *lower* limit MACHO halo fraction $f_{\rm M,low}$, rather than with the central value $f_{\rm M}$ as in Paper I. This latter difference is particularly important because it enlarges both the sizes of the dynamically-permitted region and the MACHO plateau, and hence enlarges their intersection. Since these differences serve to maximise the size of the surviving region, the constraints shown in this paper should be taken as *firm* limits on allowed cluster parameters.

4. Constraints on cluster membership

Figure 1 assumes that all stars reside in clusters at the present day, an unrealistic assumption since one expects some fraction of the clusters to have evaporated away over time. As in Paper I one can place limits on the fraction of stars $f_{\rm c}$ which must remain in clusters by using the strong limits $f_{\rm max}$ on the unclustered scenario (listed in Table 2). Assuming the lower limit on the cluster halo fraction to be given by the lower limit inferred by MACHO, $f_{\rm M,low}$, the present-day halo fraction in stars which have evaporated away from clusters is $f_{h,*} > (1 - f_{\rm c})f_{\rm M,low}$. Since HST observations demand $f_{h,*} \leq f_{\rm max}$ one has

$$f_{\rm c} > 1 - (f_{\rm max}/f_{\rm M,low}). \qquad (4)$$

The resulting values for $f_{\rm c}$ for 0.2-$M_\odot$ and 0.092-$M_\odot$ stars are given in Table 3.

Table 3. Microlensing halo fractions and minimum clustering fractions for the reference halo models. Column 2 gives the expected optical depth for a full halo as calculated by Alcock et al. (1996). Column 3 gives the central value for the halo fraction using the 1st+2nd year optical depth estimate of 2.94×10^{-7} measured by Alcock et al. (1997), and subtracting from it an optical depth of 5×10^{-8} expected from non-halo populations. The 4th column gives the 95% CL lower limit on the halo fraction using the lower limit for the measured optical depth of 1.47×10^{-7}. The last two columns give the lower limit on the present-day clustering fraction using column 4, Eq. 4 and Table 2.

| Model | $\tau_{\rm exp}/10^{-7}$ | $f_{\rm M}$ | $f_{\rm M,low}$ | $f_{\rm c}$ | |
				0.2 $M_\odot$	0.092 $M_\odot$
A	5.6	0.43	0.17	0.995	0.96
B	8.1	0.30	0.12	0.995	0.96
C	3.0	0.81	0.32	0.995	0.97
D	6.0	0.41	0.16	0.994	0.97
S	4.7	0.52	0.21	0.994	0.95

From Table 3 it is clear that all models require a very high fraction of all stars to reside in clusters at present.

Even for hydrogen-burning limit stars the required clustering fraction must be at least 95% at present. Capriotti & Hawley (1996) have undertaken a detailed analysis of cluster mass loss within an isothermal halo potential for a range of cluster masses, density profiles and Galactocentric distances. Their analysis takes account of evaporation, disruption and tidal processes. They find that clusters with masses between $10^5 - 10^7$ $M_\odot$ generally survive largely intact to the present day but that less massive clusters survive only if they have high central density concentrations, nearly circular orbits and reside at large distances from the Galactic centre. At the Solar position Capriotti & Hawley find that clusters with a half-mass to tidal radii ratio of 0.3 (comparable to the value for the clusters analysed here and in Paper I) survive more than 95% intact only if they have masses exceeding 10^6 $M_\odot$.

However, there are a number of reasons why these limits may be stronger than applicable to the low-mass star cluster scenario. Firstly, Capriotti & Hawley assume that the clusters comprise $m = 0.8$ $M_\odot$ stars (i.e. between 4 and 9 times more massive than the stars considered in the present study). The evaporation timescale scales approximately as m^{-1} for a fixed cluster mass, so for clusters comprising lower mass stars the evaporation timescale is correspondingly longer. Secondly, the local halo density assumed by Capriotti & Hawley of 0.0138 $M_\odot$ pc^{-3} at a Galactocentric distance of 8.5 kpc is on the higher end of the values for the halo models analysed in this paper, and is considerably larger than the allowed MACHO lower limit, $f_{\rm M,low}\rho_0$, on the local density in lenses (by a factor of between 5 and 10 after normalising to a distance $R_0 = 8$ kpc). Hence disruption due to close encounters with other clusters is substantially less in the halo models investigated here than for the model analysed by Capriotti & Hawley.

Lastly, a study by Oh & Lin (1992) has shown that the cluster escape rates may be substantially smaller than commonly assumed due to angular momentum transfer arising from the action of the Galactic tidal torque on cluster stars with highly eccentric orbits (which in the absence of the torque would constitute the bulk of the escapees). The rates calculated by Oh & Lin for isotropic cluster models are broadly consistent with the values used by Capriotti & Hawley (1996) and other authors, but for the case of anisotropic stellar orbits the escape rates can be 1–2 orders of magnitude smaller, again implying correspondingly longer evaporation timescales. It therefore appears that, under certain conditions, one may be able to reconcile the high cluster fraction requirements derived in the present study with the findings of cluster dynamical studies, at least for clusters comprising stars close to the hydrogen-burning limit.

In any case, the validity of the figures in Table 3 depend upon just how smoothly distributed are the stars which have evaporated from clusters. If they still have not completely homogenised today, instead maintaining a

somewhat lumpy distribution (reflecting their cluster origin), then the limits on f_c are too strong.

For example, a cluster with a mass 3×10^4 M$_\odot$ and radius 3 pc represents an over-density of about 3×10^4 over the background average at the Solar neighbourhood [i.e $\delta\rho/\rho \equiv (\rho - \overline{\rho})/\overline{\rho} = 3 \times 10^4$]. However, an under-density in the unclustered (or more precisely 'post-clustered') stellar population of just a factor 10 ($\delta\rho/\rho = -0.9$) over volumes larger than 3×10^5 pc^3, which is roughly the volume probed by 50 HST fields for hydrogen-burning limit stars (and is of order 10 times smaller than the halo volume per cluster), is all that is required to weaken the constraints on $f_{\max}$ by a factor 10. This would result in a much more comfortable lower limit on f_c of just 0.5 for 0.092-M$_\odot$ stars, rather than 0.95. If the under-density is a factor 5 lower than the background ($\delta\rho/\rho = -0.8$) one requires $f_c > 0.75$ for the lowest mass stars and for an under-density factor of 2 ($\delta\rho/\rho = -0.5$) f_c must exceed 0.9.

In order to rule out the cluster scenario definitively (say with 95% confidence) one needs a survey that is both sufficiently wide and deep that it might be expected to contain at least 3 clusters on average, regardless of their mass and radius (though their mass and radius must be dynamically permitted). From Fig. 1 it appears that the most difficult dynamically-allowed clusters for HST to exclude are those with a mass of around 3×10^4 M$_\odot$. If the halo fraction in low-mass stars is around 40%, typical of the preferred value for the MACHO results, then the local number density of such clusters is around 130 kpc^{-3} (adopting a local halo density of 0.01 M$_\odot$ pc^{-3}; in reality of course the average density within the fields is dependent upon the halo model and the field locations). If the clusters comprise hydrogen-burning limit zero-metallicity stars ($V - I = 1.57$) then a HST-type survey will be sensitive to them out to about 3.6 kpc in the I band [using the colour-magnitude relation of Eq. (3), and assuming a limiting I-band sensitivity of 24 mag], so in order to expect to detect at least 3 such clusters, the survey must cover a solid angle of at least 4.5 deg^2, or the equivalent of 3 700 HST fields! Therefore, only if HST fails to detect any clusters from 3 700 fields would dynamically-allowed clusters be ruled out with 95% confidence from explaining all of the observed microlensing events. For comparison, an all-sky K-band survey over Galactic latitudes $|b| > 10°$ requires a limiting magnitude of about 17.5 in order to produce similar constraints. This should be compared to the expected K-band limit of about 14 for the ground-based DENIS and 2MASS surveys.

An easier alternative is to instead obtain several fields as close to the Galactic centre as is feasible, where the dynamical constraints are much stronger than for the Solar neighbourhood position. For low-mass stars, this necessitates a telescope such as HST with the capability for obtaining very deep fields, since shallow surveys with wide angular coverage essentially only probe the local Solar neighbourhood.

5. Conclusion

Kerins (1997), referred to as Paper I, has suggested that low mass stars could provide the substantial dark matter fraction indicated by the combined 1st- and 2nd-year MACHO gravitational microlensing results. Whilst observations from Hubble Space Telescope (HST) and other instruments have been interpreted as excluding such stars from having a significant halo density, Paper I shows that their density could in fact be substantial if they are grouped into globular-cluster configurations. The motivation for such clusters comes from the baryonic dark matter formation scenarios which are discussed in Paper I. Paper I calculates the constraints on such clusters (assuming they comprise low-mass stars of primordial metallicity) which arise from MACHO microlensing results, dynamical constraints on massive halo objects, and observations from 20 HST fields obtained by Gould et al. (1996). However, the results of Paper I apply only to the spherically-symmetric cored isothermal halo model investigated there.

In the present study, the number of HST fields utilised has been increased to 51, and now incorporates the Hubble Deep Field and Groth Strip fields (Gould et al. 1997). The model dependency of the results in Paper I has been tested by adopting 5 of the reference halo models employed in the MACHO collaboration's analysis of its microlensing results. One of the models is similar to the halo investigated in Paper I whilst the other 4 are drawn from a self-consistent family of power-law halo models and comprise spherically-symmetric haloes with a rising rotation curve, a falling rotation curve and a flat curve, as well as a flattened (E6) halo model.

The 51 HST fields contain just 145 candidates with $V - I$ colours between 1.2 and 1.7 (spanning the colour range predicted for zero-metallicity stars with masses between the hydrogen-burning limit and 0.2 M$_\odot$) against the tens or hundreds of thousands predicted for the halo models. From this one concludes that the halo fraction in unclustered low-mass stars is at most $0.5 - 1.1\%$ with 95% confidence, depending on the halo model, and in all cases falls well short of providing even the lower-limit halo fraction inferred by MACHO.

However, in the cluster scenario there exists a wide range of cluster masses and radii which can allow a halo fraction consistent with the lower limit derived from MACHO microlensing results whilst remaining compatible with dynamical limits and HST observations. Consistency with the preferred microlensing halo fraction, rather than the lower limit, requires fine tuning of the cluster parameters (as found in Paper I), but is possible for all models investigated.

The one potentially serious problem for the cluster scenario is that the strong constraints on unclustered stars imply that an overwhelming fraction of all stars, at least 95%, must still reside in clusters at the present day. This is higher than expected from generic cluster evaporation

considerations for much of the permitted cluster mass range, though it may still be consistent with clusters comprising stars with anisotropic orbits. In any case, these limits assume that stars which have already evaporated from clusters now form a perfectly smooth distribution which traces the halo density profile. If instead these stars still have a lumpy distribution, reflecting the fact that they previously resided in clusters, then the cluster fraction limits are too strong.

Probably the only way to definitively exclude or confirm the cluster scenario is to obtain several deep fields as close to the Galactic centre as is practical, where the strong dynamical constraints severely restrict the range of feasible cluster parameters.

References

Adams, F. C., Laughlin, G., 1996, ApJ, 468, 586
Alcock, C. et al., 1996, ApJ, 461, 84
Alcock, C. et al., 1997, ApJ, in press
Axelrod, T., 1997, seminar given at the Aspen Center for Physics summer workshop: "Microlensing, dark matter & Galactic structure", Aspen Colorado, May 26th – June 13th
Bahcall, J. N., Flynn, C., Gould, A., 1992, ApJ, 389, 234
Bahcall, J. N., Flynn, C., Gould, A., Kirhakos, S., 1994, ApJ, 435, L51
Burstein, D., Heiles, C., 1984, AJ, 90, 817
Capriotti, E. R., Hawley, S. L., 1996, ApJ, 464, 765
Carr, B. J., 1994, ARA&A, 32, 531
Carr, B. J., Bond, J. R., Arnett, W. D., 1984, ApJ, 277, 445
Carr, B. J., Lacey, C. G., 1987, ApJ, 316, 23
Carr, B. J., Sakellariadou, M., 1997, ApJ, submitted
Chabrier, G., Segretain, L., Méra, D., 1996, ApJ, 468, L21
Evans, N. W., 1994, MNRAS, 267, 333
Flynn, C., Gould, A., Bahcall, J. N., 1996, ApJ, 466, L55
Gould, A., Bahcall, J. N., Flynn, C., 1996, ApJ, 465, 759
Gould, A., Bahcall, J. N., Flynn, C., 1997, ApJ, 482, in press
Graff, D. S., Freese, K., 1996, ApJ, 456, L49
Graff, D. S., Laughlin, G., Freese, K., 1997, ApJ, submitted
Kerins, E. J., 1997, A&A, 322, 709 (Paper I)
King, I. R., 1962, AJ, 67, 471
Kuijken, K., Gilmore, G., 1989, MNRAS, 239, 651
Lacey, C. G., Ostriker, J. P., 1985, ApJ, 299, 633
Moore, B., 1993, ApJ, 413, L93
Moore, B., Silk, J., 1995, ApJ, 442, L5
Oh, K. S., Lin, D. N. C., 1992, ApJ, 386, 519
Renault, C. et al., 1997, A&A, in press
Ryu, D., Olive, K. A., Silk, J., 1990, ApJ, 353, 81
Saumon, D., Bergeron, P., Lunine, J. I., Burrows, A., 1994, ApJ, 424, 333

Model C

Model D

Model S